Received: 9 April 2018 | Revised: 18 June 2018 | Accepted: 12 July 2018

DOI: 10.1111/ffe.12900

ORIGINAL CONTRIBUTION

WILEY

An analytically formulated structural strain method for fatigue evaluation of welded components incorporating nonlinear hardening effects

Xianjun Pei | Pingsha Dong

Department of Naval Architecture and Marine Engineering, University of Michigan, Ann Arbor, MI 48109, USA

Correspondence
P. Dong, Department of Naval Architecture and Marine Engineering, University of Michigan, Ann Arbor, MI 48109, USA.
Email: dongp@umich.edu

Funding information
Traction Power National Key Laboratory, Grant/Award Number: TPL 1605; National Research Foundation of Korea, Grant/Award Number: GCRC-SOP; ONR, Grant/Award Number: N00014-10-1-0479

Abstract

An analytically formulated structural strain method is presented for performing fatigue evaluation of welded components by incorporating nonlinear material hardening effects by means of a modified Ramberg-Osgood power law hardening model. The modified Ramberg-Osgood model enables a consistent partitioning of elastic and plastic strain increments during both loading and unloading. For supporting 2 major forms of welded structures in practice, the new method is applied for computing structural strain defined with respect to a through-thickness section in plate structures and cross section in piping systems. In both cases, the structural strain is formulated as the linearly deformation gradient on their respective cross sections, consistent with the "plane sections remain plane" assumption in structural mechanics. The structural strain-based fatigue parameter is proposed and has been shown effective in correlating some well-known low-cycle and high-cycle fatigue test data, ranging from gusset-to-plate welded plate connections to pipe girth welds.

KEYWORDS

low-cycle fatigue, structural strain method, modified Ramberg-Osgood model, mesh-insensitive method, stress concentration

1 | INTRODUCTION

Fatigue evaluation of welded components has always been challenging because of the presence of various forms of geometric discontinuities such as sharp notches at weld locations, which introduce stress and/or strain singularity, leading to mesh size sensitivity in finite element (FE) calculations and strain gauge size/location sensitivity in experimental measurements.[1] Historically, there are several approaches for mitigating some of these issues in stress determination. These include nominal stress approach,[2,3] surface extrapolation-based hot spot stress approach,[4,5] equivalent notch radius-based local stress or strain approach,[6,7] and more recently mesh-insensitive traction structural stress method which is also referred to as master S-N curve method.[8]

σ, Stress; M_a, Moment amplitude; F_a, Force amplitude; I, Moment of inertia; L, Length of pipe; R, Radius of pipe; ε_s, Structural; ε_m, Membrane part of structural strain; ε_b, Bending part of structural strain; k, Slope to determine structural strain; b, Intercept to determine structural strain; σ_s, Structural stress; σ_m, Membrane part of structural stress; σ_b, Bending part of structural stress; E, Young's modulus of material; α, m, σ_0, Material constant of Ramberg-Osgood Equation; σ_{prop}, Proportional limit of material; r, $r = \sigma_{prop}/\sigma_0$; ε^p, Plastic strain in uniaxial stress state; $\bar{\varepsilon}^p$, Equivalent plastic strain in tri-axial stress state; $\boldsymbol{\varepsilon}^{\mathbf{p}}$, Plastic strain tensor in tri-axial stress state; σ_i, Stress of i^{th} component; ε_i, Strain of i^{th} component; $\boldsymbol{\varepsilon}^{\mathbf{e}}$, Elastic strain tensor; $\boldsymbol{\varepsilon}^{\mathbf{total}}$, Total strain tensor; f, Yield function; γ, Plastic multiplier; M, Moment

Nominal stress approach, also referred to as weld classification method[2] or weld category method,[9] limits its applications to simple components subjected to simple loading conditions, on which strength of materials theory can be reasonably applied for nominal stress determination. In addition, a proper selection of an applicable S-N curve out of many requires judgment call. The surface extrapolation approach assumes that weld toe stress can be represented by a hot spot stress definition obtained using an extrapolated stress to a weld location (eg, at weld toe) from specified surface positions, eg, at 0.4t and 1t (t: plate thickness) from weld toe position. Such a hot spot stress definition seems not immune to mesh size sensitivity [eg, 1,8], in addition to its lack of a well-argued mechanics basis. A similar argument can be made regarding equivalent notch stress method by assuming a radius, such as using 0.05 mm for thin-walled welded structures[10,11] and 1 mm for typical steel and aluminium weldments.[12,13]

As for the mesh-insensitive traction structural stress method, it was formulated by imposing equilibrium conditions through a novel use of nodal forces and moments available from FE output[1] and shown to provide a consistent stress concentration characterization for differentiating effects of different joint types and loading conditions[1,8] on fatigue behaviours. Its relevance to fracture mechanics-based traction stress definition enabled the development of master S-N curve by collapsing a large amount of fatigue test data obtained from various joint geometries, loading modes, and plate thicknesses into a narrow band,[8,14] which has been adopted by ASME Section VIII Division 2 Code since 2007.[8] The method has been shown capable of correlating multiaxial test data[15] as well as some low-cycle fatigue test data[16] in piping components. Regarding the latter, Dong et al[16] analyzed a series of low-cycle fatigue tests of girth welded pipes including some well-known tests performed by Markl[17] and more recently by Scavuzzo et al[18] under displacement-controlled conditions (see Figure 1). Dong and Yang[19] investigated a large amount of girth-welded umbilical tubes subjected to large deformation reeling/unreeling conditions. Both studies have showed that the low-cycle fatigue test data analysed falls onto the same master S-N curve scatter band as high-cycle fatigue data if a pseudoelastic nominal load (F_a) or nominal stress is available from a load-displacement plot, as illustrated in Figure 1C.

The pseudoelastic load method shown in Figure 1B, C dates back to Markl's work[17] which has since been used as a basis for low-cycle fatigue design in ASME Codes and Standards.[20] Consider either cantilever beam bending or 4-point beam bending cyclic fatigue tests, a cyclic loading was accomplished by imposing a constant displacement amplitude (δ_a). The corresponding actual load amplitude the component experienced should be F_m, measured from a load cell reading. For low-cycle fatigue analysis, where the structure beyond yield limit, a pseudoelastic load F_a was obtained by extrapolating the linear portion of the stabilized load-displacement curve up to the specified applied displacement amplitude (δ_a) (see Figure 1C). The pseudoelastic nominal stress is then calculated by a simple elastic beam bending formula under the pseudoelastic load:

$$\sigma = \frac{M_a}{I}R \qquad M_a = F_a L \tag{1}$$

Here, R and I are outer radius and moment of inertia of the pipe, respectively, while M_a is the moment corresponding to the pseudoelastic load. As shown in Dong et al[16] and also demonstrated in Figure 1D, as long as such a load-displacement curve is available, the pseudoelastic stress representation of low-cycle fatigue data provides a demonstrated transferability between low-cycle and high-cycle fatigue regime, as shown in Figure 1D. One major limitation is that it cannot be used for low-cycle fatigue evaluation under load-controlled

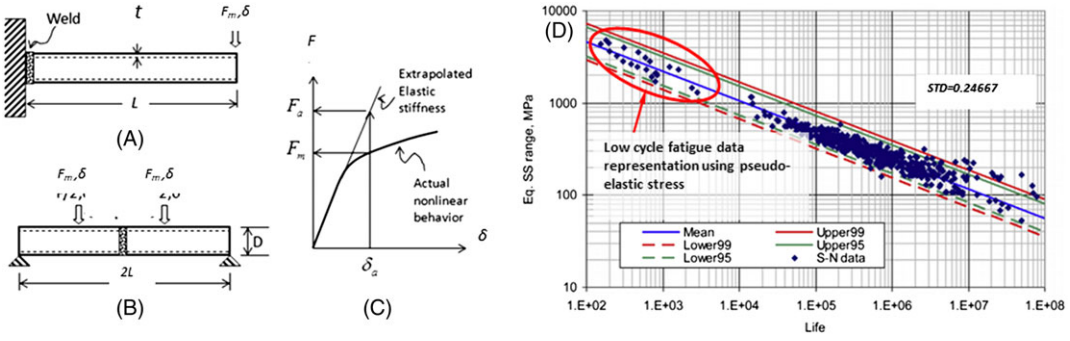

FIGURE 1 Original pseudoelastic stress concept by Markl for analyzing fatigue test data of pipe sections: A, cantilever bending, B, 4-point bending, C, pseudoelastic stress determination using extrapolated pseudoelastic load using measured load-displacement curve, and D, fatigue data analysis results using pseudoelastic structural stress [Colour figure can be viewed at wileyonlinelibrary.com]

conditions without a relevant load-displacement curve. The other is that for more complex structural components other than pipes, there exists no characteristic load-displacement curve, eg, a flat head vessel under high amplitude of cyclic pressure loading conditions.

The pseudoelastic stress calculation procedure given in Equation (1) implies that the assumption that "a plane of beam section remains as a plane during deformation" continues to be valid at weld location in elastic-plastic deformation regime, at least for fatigue characterization purpose. Equivalently, it suggests that the linear deformation gradient across the whole pipe section can be used to correlate fatigue test data, rather than relying on localized notch strains induced by weld geometric discontinuities, which are, to a large extent, already contained in the test data when test components represent typical weld quality and weld bead geometric characteristics. The use of linear strain gradient across a pipe section or a plate through-thickness section is consistent with the traction-based structural stress definition within linear elastic deformation context, which is determined in through-thickness membrane and bending parts at any given weld location by imposing equilibrium conditions in both through-thickness and along weld line.[1,8] It is this connection that has led to the recent developments of structural strain method (see Gas Transmission and Distribution Piping Systems,[21] Pei et al,[22] and Dong et al[23]) for extending the existing traction structural stress method to applications in low-cycle fatigue regime with some degree of success, eg, under the assumption of elastic perfectly plastic material without considering any strain hardening effects. Along this line, the treatment of low-cycle fatigue for welded plate components is given in Dong et al[21] and for pipe components in Pei et al.[22] Note that in Dong et al,[21] a series of low-cycle fatigue tests of plate joints were analyzed by using a structural strain procedure that approximately takes into account strain hardening effects because of cross section yielding conditions encountered in fatigue testing.

The purpose of this paper is to present a generalized structural strain method that is applicable for fatigue evaluation of both welded plate structures and pipe components by incorporating a more general Ramberg-Osgood strain hardening law so that load-controlled conditions can be effectively treated. The reason for making a distinction between plate and pipe components is that "plane-remaining-plane" conditions is imposed with respect to plate thickness in plate components while the same condition is imposed with respect to the entire pipe section in pipe components. The latter is to be consistent to how fatigue tests have been performed and fatigue failure criteria have been defined historically for piping systems within ASME community.[24] In addition, piping system stress analysis is typically done with beam element models[20] which is consistent with the structural strain definition across a pipe section.

The paper is organized as follows. After introducing the definition of structural strain, analytical formulations governing structural strain development are presented for plate and pipe sections subjected to remote membrane and bending stresses in Section 2. In addition, a modified Ramberg-Osgood power law hardening model is presented for facilitating a consistent elastic and plastic strain partitioning which is required for calculating elastic core size that can be directly related to the cross-sectional plane as a result of elastic-plastic deformation. A robust numerical procedure is then presented for solving the analytically formulated governing equations in Section 3, along with a series of calculation examples for validating the structural strain results obtained from the analytical formulation and by direct finite element computations. Then, low-cycle fatigue test data from both welded plate and pipe components are analyzed using the structural strain method developed for demonstrating its effectiveness. Finally, relative contributions to structural strain developments as a result of plane-strain conditions and material hardening effects are discussed in Section 5, particularly on how the structural strain calculation procedures may be further simplified if power law hardening parameters may be not available for fatigue evaluation of welded components in practice.

2 | STRUCTURAL STRAIN DEFINITION AND FORMULATION

2.1 | Structural strain definition

Consider a fillet-welded plate structure with a representative cross section shown in Figure 2A. Without losing generality, a weld toe fatigue cracking into plate thickness, ie, along plane A-A, is considered as shown. Although local stress along the hypothetical crack plane can be highly nonlinear, the corresponding traction structural stress component (ie, opening stress component with respect crack plane A-A) can be calculated in a mesh-insensitive manner[1,8] in normal membrane part (σ_m) and normal bending part (σ_b) under specified remote loading conditions. Then, an equivalent 2D plate section problem can be described as shown in Figure 2B, subjected to the same statically equivalent membrane (σ_m) and bending stress (σ_b) that can be expressed as force N and moment M per unit length. The resulting linear strain distribution (linear deformation gradient) in membrane strain ε_m and bending strain ε_b is defined as structural strain, after imposing both equilibrium conditions

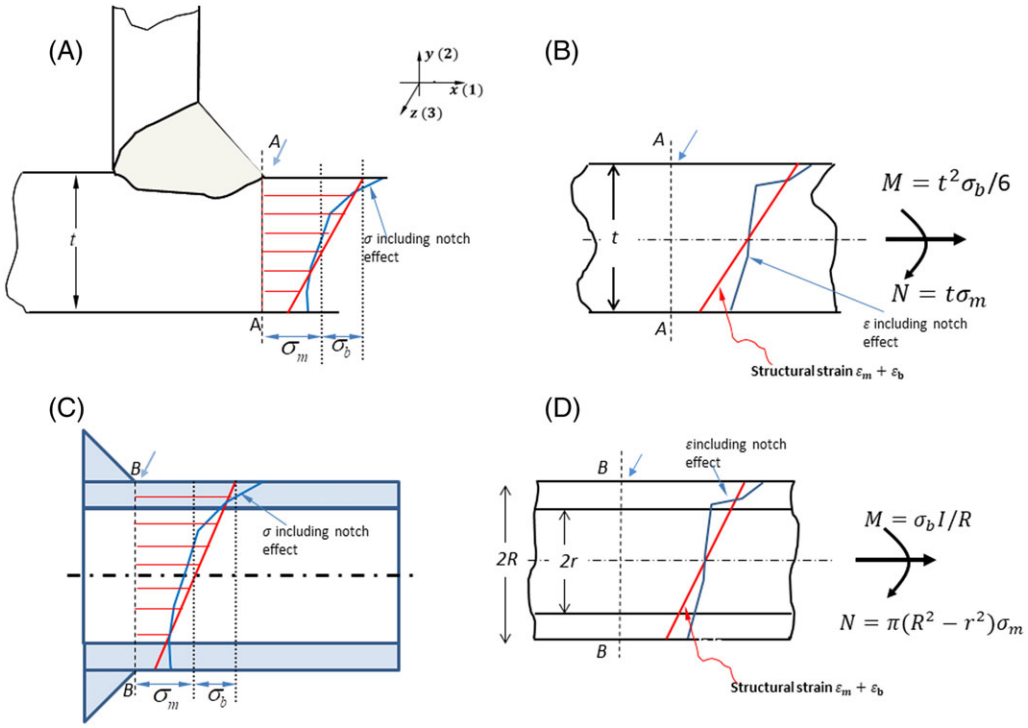

FIGURE 2 Structural strain definitions: A, traction structural stress ($\boldsymbol{\sigma_m,\sigma_b}$) determined on a plate cross-sectional A-A using mesh-insensitive method, [1,8] B, structural strain ($\boldsymbol{\varepsilon_m + \varepsilon_b}$) at along plate section A-A, C, traction structural stress ($\boldsymbol{\sigma_m,\sigma_b}$) on pipe cross-sectional B-B obtained from finite beam element analysis, and D, structural strain ($\boldsymbol{\varepsilon_m + \varepsilon_b}$) at along pipe section B-B [Colour figure can be viewed at wileyonlinelibrary.com]

and material yield criteria. Similarly, the structural strain with respect to pipe cross section at weld toe position in Figure 1C acting on plane B-B can be described as shown in Figure 2D. This structural strain definition is consistent with the traction structural stress definition by suppressing strain singularity at weld toe or weld root.

The structural strain in $\varepsilon_m, \varepsilon_b$ shown in Figure 2B, D can be written as a linear deformation gradient described as:

$$\varepsilon_s(y) = \varepsilon_m + \varepsilon_b = ky + b \tag{2}$$

Under general loading conditions, as shown in Dong,[1] 3 traction structural stress components are available and can be extracted in a mesh-insensitive manner on a given hypothetical crack plane, eg, A-A in Figure 2A or B-B in Figure 2C. These are normal traction structural stress (σ_m,σ_b) contributing to mode I loading and 2 shear traction structural stresses (τ_m^{II}, τ_b^{II} and $\tau_m^{III}, \tau_b^{III}$) contributing to modes II and III loading, respectively. The corresponding structural strain definitions can be expressed as:

$$\begin{aligned} \varepsilon_m^{I,II,III} &= \frac{\varepsilon_{\max}^{I,II,III} + \varepsilon_{\min}^{I,II,III}}{2} \\ \varepsilon_b^{I,II,III} &= \frac{\varepsilon_{\max}^{I,II,III} - \varepsilon_{\min}^{I,II,III}}{2} \\ \varepsilon_s^{I,II,III} &= \varepsilon_m^{I,II,III} + \varepsilon_b^{I,II,III} \end{aligned} \tag{3}$$

Here, $\varepsilon^{I,\ II,\ III}$ corresponds to structural strain components on a hypothetical crack plane subjected to modes I, II, and III loading conditions. Without losing generality, hereafter it is assumed that only the normal structural strain component (ε^I) is dominant. (Other 2 components can be treated in exactly the same manner.) A simplified notation can then be used, eg, using ε_m for representing ε_m^I, ε_b for ε_b^I, and ε_s for ε_s^I.

2.2 | Formulation

2.2.1 | Material hardening behaviour

In 2 related studies, Dong et al[21] and Pei et al[22] adopted elastic perfectly plastic material model in determining structural strains at weld locations in plate and pipe components, such that solutions can be expressed in a closed form in elastically calculated traction structural stresses. Their results indicate an improvement in test data correlation. However, once plastic deformation becomes severe or elastic core size becomes small, elastic perfectly plastic material model can significantly overestimate structural strain without considering strain-hardening effects, particularly when membrane stress σ_m becomes dominant. To overcome this issue and introduce a more general treatment of material hardening behaviors, a modified Ramberg-Osgood constitutive relation is presented here,

which allows a clear partitioning of elastic and plastic strain increments while maintaining the same power law structure as its original form.

The original Ramberg-Osgood relation was first proposed by Ramberg and Osgood,[25] which provides a rather versatile representation of material stress-strain relations for numerous metals and is widely adopted by engineering community.[26-28]The relation describes nonlinear material behaviour in total strain:

$$\varepsilon = \frac{\sigma}{E} + \alpha\frac{\sigma_0}{E}\left(\frac{\sigma}{\sigma_0}\right)^m \tag{4}$$

in which ε is the total strain, E is Young modulus, and α, m, and σ_0 are material parameters obtained in a power law fit of true stress strain curve. Two major deficiencies exist in the original Ramberg-Osgood relation given in Equation (4): (1) the power term in the equation implies that material exhibits nonlinear deformation behaviour even when applied stress σ is well below material nominal yield strength, often referred to as nonlinear elasticity material model, and (2) the equation form does not allow a clear separation of elastic and plastic deformations. As a result, linear-elastic unloading behaviour and plastic strain accumulation cannot be consistently modelled when dealing with cyclic fatigue loading conditions when incremental plasticity theory is invoked. The former is a prerequisite for determining component cross-sectional elastic core size.

To overcome the above 2 deficiencies, a modified Ramberg-Osgood equation is proposed as follows:

$$\varepsilon = \begin{cases} \varepsilon^e = \dfrac{\sigma}{E} & \left(\sigma \le \sigma_{prop}\right) \\ \varepsilon^e + \varepsilon^p = \dfrac{\sigma}{E} + \alpha\dfrac{\sigma_0}{E}\left[\left(\dfrac{\sigma}{\sigma_0}\right)^m - r^m\right] & \left(\sigma > \sigma_{prop}\right) \end{cases} \tag{5}$$

Here, σ_{prop} is the proportional limit of the material and r is defined as

$$r = \frac{\sigma_{prop}}{\sigma_0} \tag{6}$$

which is the ratio of material proportional limit σ_{prop} over reference stress σ_0. The detail explanation of Equation (5) is given in Appendix A. The modified Ramber-Osgood equation given in Equation (5) enables a clear separation of material elastic strain from plastic strain, and provides a convenient form for expressing strain hardening effect in plastic strain, ie,

$$\sigma = \sigma_0\left(\frac{E\varepsilon^p}{\alpha\sigma_0} + r^m\right)^{1/m} \tag{7}$$

In dealing with multiaxial stress state, ε^p in Equation (7) can be replaced by $\bar{\varepsilon}^p$ which is the equivalent plastic strain given by

$$\bar{\varepsilon}^p = \left(\frac{2}{3}\boldsymbol{\varepsilon}^{\mathbf{p}}:\boldsymbol{\varepsilon}^{\mathbf{p}}\right)^{1/2} \tag{8}$$

in which $\boldsymbol{\varepsilon}^{\mathbf{p}}$ is the plastic strain tensor.

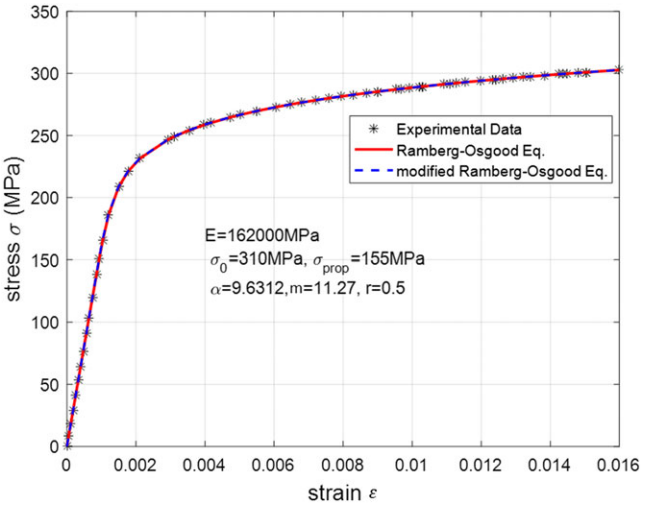

FIGURE 3 Comparison of the original Ramberg-Osgood and the modified Ramberg-Osgood fits for representing stainless steel 304 stress-strain data [Colour figure can be viewed at wileyonlinelibrary.com]

To demonstrate the effectiveness of Equation (5) in representing experimental stress-strain test data, eg, stainless steel 304, Figure 3 compares the fitting results between the original Ramberg-Osgood equation (Equation (4)) and the modified Ramberger-Osgood equation (Equation (5)) with experimental data. There is no noticeable difference in the fitting results shown in Figure 3. The introduction of a proportional limit in the form of Equation (5) allows the partitioning of total strain in elastic and plastic strain components, which enables the determination of structural strain according to the definitions given in Section 2.1.

2.2.2 | Plate section

Consider a welded plate component shown in Figure 4, in which the highest stress concentration location is as shown when the component is loaded in remote tension or bending on the base plate. By performing the traction structural stress analysis using method provided in Dong[1] and Dong et al,[8] the structural stress σ_s can be calculated on the curvilinear cut along the entire weld line into base plate thickness (Figure 4B) in a mesh-insensitive manner. Here, $\sigma_s = \sigma_m + \sigma_b$ is the summation of membrane and bending stress component. With respect to the through-thickness section at the critical location, a 2D cross-sectional representation under plane strain conditions is

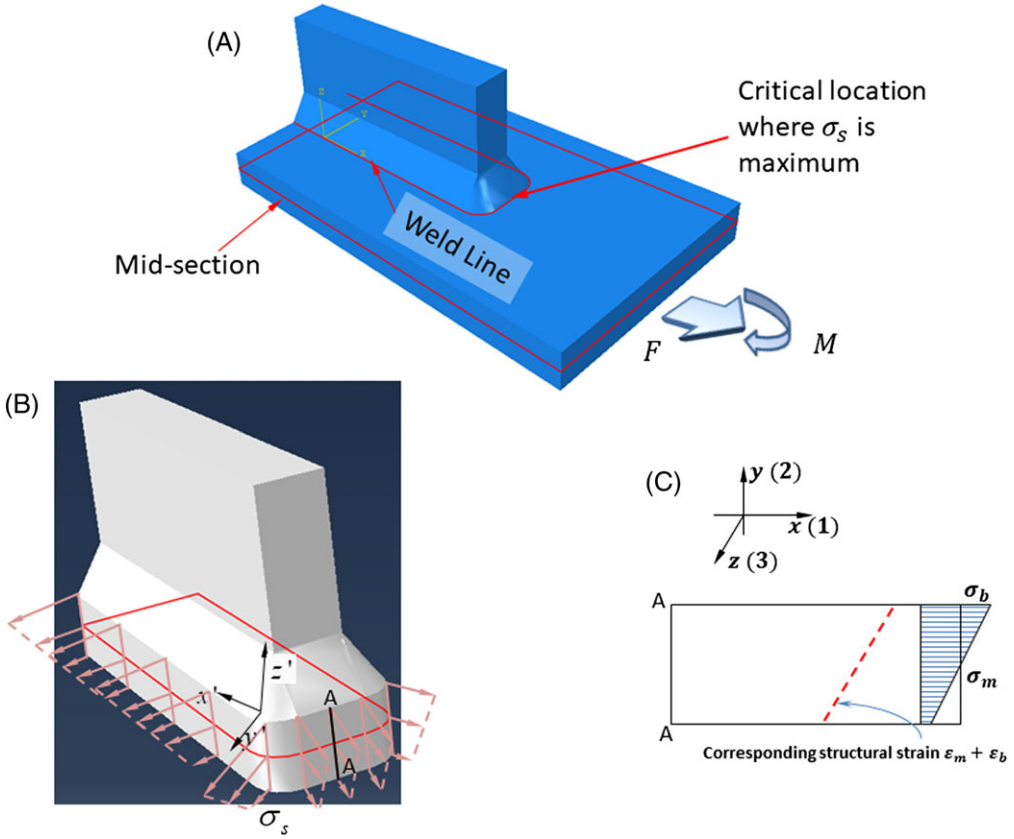

FIGURE 4 Traction structural stress determination using mesh-insensitive method given in Dong[1] and Dong et al[8]: A, welded plate component under remote loading, B, illustration of traction stress distribution on curvilinear cut at weld toe line into plate thickness, and C, structural strain at critical through-thickness section A-A corresponding to traction structural stress (σ_m,σ_b) [Colour figure can be viewed at wileyonlinelibrary.com]

shown in Figure 4C, for which σ_m and σ_b serve as statically equivalent remote load. The corresponding structural strain should satisfy equilibrium conditions, and material constitutive relation represented by the modified Ramberg-Osgood relation described in the proceeding section. Then, the equilibrium equations are:

$$\begin{aligned} \int_{-t/2}^{t/2} \sigma_1(y)dy &= \sigma_m t \\ \int_{-t/2}^{t/2} \sigma_1(y)ydy &= \int_{-t/2}^{t/2} \left(\frac{2\sigma_b}{t}y\right)ydy = \frac{\sigma_b t^2}{6} \end{aligned} \tag{9}$$

Here, $\sigma_1(y)$ is the normal stress in x direction, ie, axis 1 direction. The deformation gradient across plate thickness must be linear to be consistent with the structural strain definitions in Section 2.1 and can be written as:

$$\varepsilon_1^{total}(y) = \varepsilon_1^e(y) + \varepsilon_1^p(y) = ky + b \tag{10}$$

where ε_1^{total} is the total structural strain which can be decomposed into plastic strain $\varepsilon_1^p$and elastic strain ε_1^e. The total structural strain is assumed linearly distributed through thickness, which is a generalization of Qian's theory.[29]

Elastic stress-strain relationship can be written in 3D Hooke's law form as:

$$\begin{aligned} \boldsymbol{\sigma} &= 2G\boldsymbol{\varepsilon}^{\mathrm{e}} + \lambda Tr(\boldsymbol{\varepsilon}^{\mathrm{e}})\mathbb{I} \\ \boldsymbol{\varepsilon}^{\mathrm{e}} &= \boldsymbol{\varepsilon}^{total} - \boldsymbol{\varepsilon}^{p} \end{aligned} \tag{11}$$

where $\boldsymbol{\sigma}$ and $\boldsymbol{\varepsilon}$ are stress and strain tensors, respectively, $\boldsymbol{I}$ is rank 2 isotropic tensor, $Tr(\boldsymbol{\varepsilon}^{\boldsymbol{e}})$ is the trace of elastic strain tensor, and G is material shear modulus and

$$\lambda = \frac{E\nu}{(1+\nu)(1-2\nu)} \tag{12}$$

which is termed as Lamé parameter.

When a structure undergoes plastic deformation, yield condition must be satisfied in addition to equilibrium and linear deformation gradient conditions, which can be expressed as, in the form of the modified Ramberg-Osgood relationship, assuming isotropic hardening and von Mises yield criterion:

$$f(\sigma_e, \bar{\varepsilon}^p) = \sigma_e - \sigma_0 \left(\frac{E\bar{\varepsilon}^p}{\alpha\sigma_0} + r^m \right)^{1/m} \tag{13}$$

in which σ_e is the von-Mises stress and $\bar{\varepsilon}^p$ is effective plastic strain given in Equation (8). f represents yield criterion.[30] It should be noticed that based on the Kuhn-Tucker complementarity condition in classical computational plasticity procedure, the yield function is not allowed to be greater than 0,[30] ie,

$$f(\sigma_e, \bar{\varepsilon}^p) \leq 0 \tag{14}$$

Associative flow rule is used here, which means the direction of the plastic strain increment is defined by $\partial f / \partial \boldsymbol{\sigma}$, ie,

$$d\boldsymbol{\varepsilon}^p = d\gamma \frac{\partial f}{\partial \boldsymbol{\sigma}} \tag{15}$$

In Equation (15), γ is the plastic multiplier and $\gamma \geq 0$ by definition, and

$$d\boldsymbol{\varepsilon}^p = d\gamma \frac{\partial f}{\partial \boldsymbol{\sigma}} = \frac{3}{2} d\gamma \frac{\boldsymbol{\sigma}'}{\sigma_e} \tag{16}$$

when von-Mises yield criterion is used. In Equation (16), $\boldsymbol{\sigma}'$ is the deviatoric stress tensor.

It is important to point out here that the structural strain distribution is fully determined by k and b in Equation (10). One of the main objectives of this work is to provide an efficient means to solve (k, b) satisfying Equations (9) to (15), which will be elaborated in Section 3.

2.2.3 | Pipe section

Piping systems are often analyzed using beam element models for extracting pipe section forces and moments at a girth-welded location, which can be treated as remote loads, as shown in Figure 5. Without loss of generality, the structure strain analysis procedure for a pipe section in Figure 5A is illustrated in Figure 5B. The remote loads in Figure 5A can be related to pipe cross-sectional membrane and bending stresses as:

$$\begin{aligned} \sigma_m &= \frac{F}{A} = \frac{F}{\pi(R^2 - r^2)} \\ \sigma_b &= \frac{MR}{I} = \frac{MR}{\pi(R^4 - r^4)/4} \end{aligned} \tag{17}$$

The corresponding equilibrium conditions can be expressed as

$$\begin{aligned} &\int_{-R}^{R} \sigma_1(x,y) l(y) dy = F = \sigma_m \pi (R^2 - r^2) \\ &\int_{-R}^{R} \sigma_1(x,y) l(y) y dy = M = \frac{\sigma_b I}{R} = \frac{\sigma_b}{R} \times \frac{\pi}{4} (R^4 - r^4) \end{aligned} \tag{18}$$

Here, $l(y)$ is the cord length perpendicular to y-axis (Figure 5C). The linear deformation gradient condition must hold here by definition, as given in Equation (10). It should be noted that linear deformation gradient is

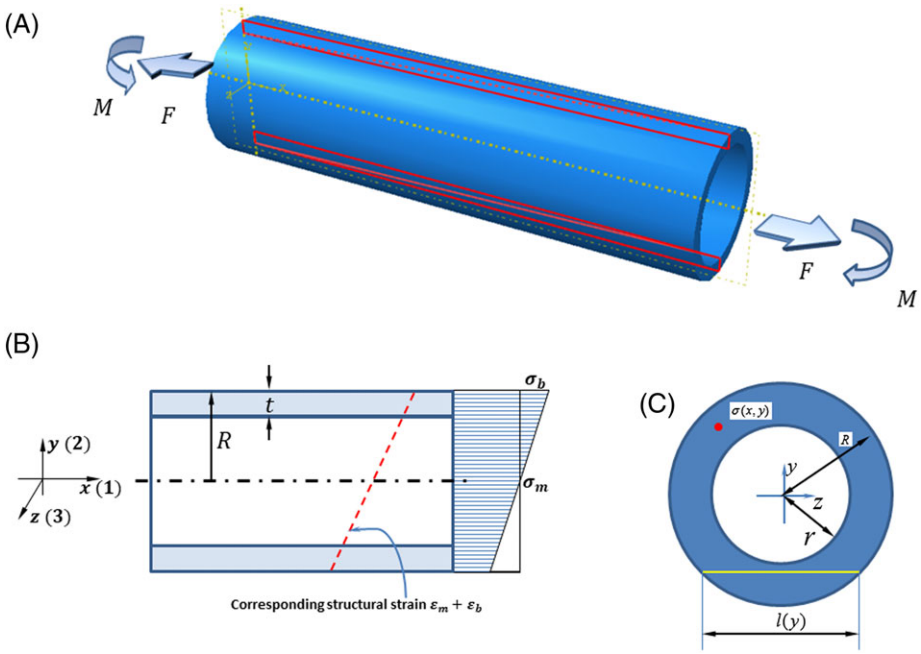

FIGURE 5 Traction structural stress determination for a pipe section in welded pipe component: A, pipe under remote loading, B, longitudinal cross section of pipe section, and C, transverse cross section [Colour figure can be viewed at wileyonlinelibrary.com]

not only valid maintained across pipe wall thickness but also across the entire pipe section, as depicted in Figure 5B in the form of structural strain distribution.

If assuming that the normal stress acting on a beam cross section in Figure 5C is the only dominant stress component, the following relations exist based on classical beam theory:

$$\begin{aligned}\sigma_1 &= E\varepsilon_1^e \\ \varepsilon_1^{total} &= \varepsilon_1^e + \varepsilon_1^p = ky + b\end{aligned} \tag{19}$$

The corresponding yield criteria and flow rule can then be simplified as:

$$f(\sigma_e, \bar{\varepsilon}^p) = |\sigma_1| - \sigma_0\left(\frac{E\bar{\varepsilon}^p}{\alpha\sigma_0} + r^m\right)^{1/m} \tag{20}$$

$$d\bar{\varepsilon}_1^p = d\gamma \times \mathrm{sign}(\sigma_1) \tag{21}$$

respectively.

Finally, k and b in Equation (19) can be solved by satisfying Equations (17) through (21) to obtain the structural strain at a weld location in a piping system.

3 | SOLUTIONS, VALIDATIONS, AND APPLICATIONS

3.1 | Numerical solution procedures

The analytical formulations developed for computing structural strain for a plate section (see Section 2.2.2) and for pipe section (see Section 2.2.3) cannot be solved in closed forms. Numerical method must be used here. In the ensuing sections, a robust numerical procedure will be presented for computing structural strains for both plate and pipe sections.

3.1.1 | Plate section

As shown in Figure 4, the 2D problem illustrated in Figure 4C can be treated as a plane strain problem, ie, $\varepsilon_3 = \varepsilon_3^e + \varepsilon_3^p = 0$. It is further assumed that the shear stress and stress normal to plate surface are negligible, ie, $\tau_{12} \approx 0$, $\sigma_2 \approx 0$. Then, Equations 11 and 12 can be written as:

$$\begin{aligned}\sigma_1 &= \frac{E\varepsilon_1}{(1-\nu^2)} - \left[\frac{E\varepsilon_1^p}{(1-\nu^2)} + \frac{\nu E\varepsilon_3^p}{(1-\nu^2)}\right]\sigma_3 \\ &= \frac{\nu E\varepsilon_1}{(1-\nu^2)} - \left[\frac{\nu E\varepsilon_1^p}{(1-\nu^2)} + \frac{E\varepsilon_3^p}{(1-\nu^2)}\right]\end{aligned} \tag{22}$$

and von-Mises effective stress becomes:

$$\sigma_e = \sqrt{{\sigma_1}^2 + {\sigma_3}^2 - \sigma_1\sigma_3} \tag{23}$$

By substituting Equation (22) into Equation (9), k and b in Equation (10) can be related to total strain components and traction stresses by:

$$\begin{aligned}Eb &= (1-\nu^2)\sigma_m + \int_{-1/2}^{1/2} E\varepsilon_1^p(y')dy' + \nu\int_{-1/2}^{1/2} E\varepsilon_3^p(y')dy' \\ Ekt &= 2(1-\nu^2)\sigma_b + 12\int_{-1/2}^{1/2} E\varepsilon_1^p(y')y'dy' + 12\nu\int_{-1/2}^{1/2} E\varepsilon_3^p(y')y'dy'\end{aligned} \tag{24}$$

in which $y' = y/t$ is the coordinate normalized by plate thickness t.

In view of von-Mises yield criterion and the associative flow rule adopted, the incremental equivalent plastic strain $d\bar{\varepsilon}^p$ and plastic multiplier γ can be related by

$$\begin{aligned}d\bar{\varepsilon}^p &= \left(\frac{2}{3}d\boldsymbol{\varepsilon}^{\mathrm{p}} : d\boldsymbol{\varepsilon}^{\mathrm{p}}\right)^{1/2} = \left(\frac{2}{3}\frac{3}{2}d\gamma\frac{\boldsymbol{\sigma}'}{\sigma_e} : \frac{3}{2}d\gamma\frac{\boldsymbol{\sigma}'}{\sigma_e}\right)^{1/2} \\ &= d\gamma\end{aligned} \tag{25}$$

Finally, when material is under plastic deformation, ($d\bar{\varepsilon}^p > 0$), $d\bar{\varepsilon}^p$ can be solved by following the consistency condition in classical plastic theory:

$$f(\sigma_e + d\sigma_e, \bar{\varepsilon}^p + d\bar{\varepsilon}^p) = 0 \tag{26}$$

To solve Equations 22 to 26, an algorithm based on a classical return mapping is implemented for calculating structural strain under traction stress σ_m and σ_b, as shown in Box 1. At the beginning of each iteration, the analysis begins with an "elastic step", that is, all plastic strains are set to be equal to the values corresponding to the previous step. Parameters k and b are then solved based on equilibrium conditions described in Equation (24). Up to step 1 in Box 1, the equilibrium conditions are met, while the Kuhn-Tucker complementarity may not be. To check the Kuhn-Tucker condition, a trial stress is calculated (note: $(\blacksquare)^{tr}$ is the trial state of $(\blacksquare)$) in step 2. In step 3, the trial stress is tested. If Kuhn-Tucker condition is satisfied, the trial state becomes the solution of the problem. Otherwise, the classical return mapping algorithm as shown in Box 2 should be applied to obtain the plastic strain increment.

Box 1 Overall algorithm to obtain structural strain for plate section under plane strain conditions

Set $\varepsilon_{1,(0)}^p(y_t') = 0, \varepsilon_{3,(0)}^p(y_t') = 0, \bar{\varepsilon}^p{}_{(0)}(y_t') = 0$

while $\left(|k_{(i+1)} - k_{(i)}| > tol \text{ or } |b_{(i+1)} - b_{(i)}| > tol \text{ or } \max\left(f_{(i+1)}^{tr}\right) > 0\right)$

1. perform "elastic step"

$$\varepsilon_1^{p,tr}(y') = \varepsilon_{1,(i)}^{p}(y'), \varepsilon_3^{p,tr}(y') = \varepsilon_3^{p}(y'), \bar{\varepsilon}^{p,tr}(y') = \bar{\varepsilon}^{p}(y')$$

$$Eb_{(i+1)} = (1-\nu^2)\sigma_m + \int_{-1/2}^{1/2} E\varepsilon_1^{p,tr}(y')dy' + \nu\int_{-1/2}^{1/2} E\varepsilon_3^{p,tr}(y')dy'$$

$$Ek_{(i+1)}t = 2(1-\nu^2)\sigma_b + 12\int_{-1/2}^{1/2} E\varepsilon_1^{p,tr}(y')y'dy' + 12\nu\int_{-1/2}^{1/2} E\varepsilon_3^{p,tr}(y')y'dy'$$

$$E\varepsilon_{1,(i+1)}(y') = Ek_{(i+1)}ty' + Eb_{(i+1)}$$

2. calculate trial stress

$$\sigma_1^{tr}(y') = \frac{E\varepsilon_{1,(i+1)}(y')}{1-\nu^2} - \left[\frac{E\varepsilon_1^{p,tr}(y')}{1-\nu^2} + \frac{\nu E\varepsilon_3^{p,tr}(y')}{(1-\nu^2)}\right]$$

$$\sigma_3^{tr}(y') = \frac{\nu E\varepsilon_{1,(i+1)}(y')}{1-\nu^2} - \left[\frac{\nu E\varepsilon_1^{p,tr}(y')}{1-\nu^2} + \frac{E\varepsilon_3^{p,tr}(y')}{1-\nu^2}\right]$$

$$\sigma_e^{tr}(y') = \sqrt{(\sigma_1^{tr})^2 + (\sigma_3^{tr})^2 - \sigma_1^{tr}\sigma_3^{tr}}$$

3. check yield criteria and Kuhn-Tucker complementarity condition

$$f^{tr}(\sigma_e^{tr}, \bar{\varepsilon}^p) = \sigma_e^{tr} - \sigma_0\left(\frac{E\bar{\varepsilon}^{p,tr}}{\alpha\sigma_0} + r^m\right)^{1/m}$$

if $f^{tr} \le 0$
    Elastic step: set $(\bullet)_{(i+1)} = (\bullet)^{tr}$
Else
    Plastic step: Proceed with return mapping algorithm (see Box 2)
End if
End while

Box 2 Return mapping algorithm for 2D plane strain problems referred to in Box 1

1. solve $\Delta\bar{\varepsilon}^p$:

$$f(\sigma_e, \bar{\varepsilon}^p) = \sigma_e - \sigma_0\left(\frac{E\bar{\varepsilon}^p}{\alpha\sigma_0} + r^m\right)^{1/m} = 0 \Rightarrow$$

$$f(\sigma_e, \bar{\varepsilon}^p) = \sigma_e^{tr} - 3G\Delta\bar{\varepsilon}^p - \sigma_0\left(\frac{E\bar{\varepsilon}^p}{\alpha\sigma_0} + r^m\right)^{1/m} = 0 \Rightarrow$$

$$f(\sigma_e, \bar{\varepsilon}^p) = \sigma_e^{tr} - 3G\Delta\bar{\varepsilon}^p - \sigma_0\left[\frac{E(\bar{\varepsilon}^p{}_t + \Delta\bar{\varepsilon}^p)}{\alpha\sigma_0} + r^m\right]^{1/m} = 0$$

$$f(\sigma_e, \bar{\varepsilon}^p) = \sigma_e^{tr} - 3G\Delta\bar{\varepsilon}^p - \sigma_0\left[\frac{E(\bar{\varepsilon}^{p,tr} + \Delta\bar{\varepsilon}^p)}{\alpha\sigma_0} + r^m\right]^{1/m} = 0$$

$$f(\sigma_e, \bar{\varepsilon}^p) = \sigma_e^{tr} - \frac{3E\Delta\bar{\varepsilon}^p}{2(1+\nu)} - \sigma_0\left[\frac{E(\bar{\varepsilon}^{p,tr} + \Delta\bar{\varepsilon}^p)}{\alpha\sigma_0} + r^m\right]^{1/m} = 0$$

solve $\Delta\bar{\varepsilon}^p$ (Newton iteration)

2. update strain and stress

$$\Delta\varepsilon_1^p = \frac{3\Delta\bar{\varepsilon}^p}{2\sigma_e^{tr}}\left(\frac{2}{3}\sigma_1^{tr} - \frac{1}{3}\sigma_3^{tr}\right)$$

$$\Delta\varepsilon_3^p = \frac{3\Delta\bar{\varepsilon}^p}{2\sigma_e^{tr}}\left(\frac{2}{3}\sigma_3^{tr} - \frac{1}{3}\sigma_1^{tr}\right)$$

$$\varepsilon_{1,(i+1)}^{p,t+\Delta t} = \varepsilon_{1,(i)}^{p} + \Delta\varepsilon_1^p$$

$$\varepsilon_{3,(i+1)}^{p,t+\Delta t} = \varepsilon_{3,(i)}^{p} + \Delta\varepsilon_3^p$$

$$\bar{\varepsilon}^p{}_{(i+1)} = \bar{\varepsilon}^p{}_{(i+1)} + \Delta\bar{\varepsilon}^p$$

$$\sigma_{1,(i+1)} = \frac{E}{(1-\nu^2)}\varepsilon_{1,(i+1)} - \left[\frac{E}{(1-\nu^2)}\varepsilon_{1,(i+1)}^{p} + \frac{\nu E}{(1-\nu^2)}\varepsilon_{3,(i+1)}^{p}\right]$$

$$\sigma_{3,(i+1)} = \frac{\nu E\varepsilon_{1,(i+1)}}{1-\nu^2} - \left[\frac{\nu E\varepsilon_{1,(i+1)}^{p}}{1-\nu^2} + \frac{E\varepsilon_{3,(i+1)}^{p}}{1-\nu^2}\right]$$

Box 2 provides a detailed implementation of classical return mapping algorithm for 2D plane strain problems with material hardening behaviours modelled by the modified Ramberg-Osgood stress-strain relation. During step 1 of Box 2, effective plastic strain increment $\bar{\varepsilon}^p$ is solved by enforcing the consistency condition given in Equation (26) in which

$$\sigma_e = \sigma_e^{tr} - 3G\Delta\bar{\varepsilon}^p \tag{27}$$

Note that the proof of Equation (27) is provided in Appendix A. After updating the plastic strain increment, Kuhn-Tucker condition is satisfied while the equilibrium conditions may have been perturbed. Additional iterations in *while loop* are then carried out to ensure that both equilibrium and Kuhn-Tucker conditions are satisfied.

The algorithms described in Box 1 and Box 2 allow a rapid determination of the structural strains at a through-thickness section of welded plate components once elastic traction stresses along a given weld line have been obtained. The structural strains can then be used for low-cycle fatigue evaluation, which will be demonstrated in 1 of the latter sections.

3.1.2 | Pipe section

To obtain structural strain in a pipe section in Section 2.2.3, as illustrated in Figure 5, the numerical procedures are similar to those given in Section 3.1.1. Because there exists only 1 dominant stress component in dealing with a pipe section, the solution process is much simpler. The corresponding numerical algorithm is summarized in Box 3, with its corresponding classical return mapping algorithm being provided in Box 4. In Box 4, it is important to note that for updating equivalent plastic strain using Equations 20 and 21, $|\sigma_1|$ can be calculated from trial stress and $sign(\sigma_1)$ is typically unknown because σ_1 is not available prior to plastic strain. However, this problem can be solved by replacing $sign(\sigma_1)$ to $\mathrm{sign}(\sigma_1^{tr})$ as shown in:

$$|\sigma_1| = \left|\sigma_1^{tr}\right| - E\Delta\bar{\varepsilon}^p \qquad \text{sign}(\sigma_1) = \text{sign}\left(\sigma_1^{tr}\right) \tag{28}$$

Note that the proof of (28) is provided in Appendix B. By following the numerical algorithms given in Box 3 and Box 4, structural strain can be determined with respect to a pipe cross section once remote traction stress conditions are prescribed by means of the mesh-insensitive method.[1]

Box 3 Overall algorithm for computing structural strain at a pipe section

Set $\varepsilon^p_{1,(0)}(y_t') = 0, \varepsilon^p_{3,(0)}(y_t') = 0, \bar{\varepsilon}^p{}_{(0)}(y_t') = 0$

while $\left(|k_{(i+1)} - k_{(i)}| > tol \text{ or } |b_{(i+1)} - b_{(i)}| > tol \text{ or } \max\left(f^{tr}_{(i+1)}\right) > 0\right)$

1. perform "elastic step"

$$\varepsilon_1^{p,tr}(y_t) = \varepsilon^p_{1,(i)}(y_t), \varepsilon_3^{p,tr}(y_t) = \varepsilon_3^p(y_t), \bar{\varepsilon}^{p,tr}(y_t) = \bar{\varepsilon}^p(y_t)$$

$$Eb_{(i+1)} = \sigma_m + \frac{\int_{-1}^{1}(E\varepsilon_1^p/\sigma_0)l(y')dy'}{\pi\left[1-(r/R)^2\right]}$$

$$Ek_{(i+1)}R = \sigma_b + \frac{\int_{-1}^{1}(E\varepsilon_1^p/\sigma_0)l(y')y'dy'}{(\pi/4)\left[1-(r/R)^4\right]}$$

$$E\varepsilon_{1,\,(i+1)}(y') = Ek_{(i+1)}Ry' + Eb_{(i+1)}$$

2. calculate trial stress

$$\sigma_1^{tr}(y') = EkRy' + Eb - E\varepsilon_1^{p,tr}(y')$$

$$f^{tr}\left(\sigma_1^{tr}, \bar{\varepsilon}^p\right) = \left|\sigma_1^{tr}\right| - \sigma_0\left(\frac{E\bar{\varepsilon}^{p,tr}}{\alpha\sigma_0} + r^m\right)^{1/m}$$

3. check yield criteria and Kuhn-Tucker complementarity condition

$$f^{tr}\left(\sigma_1^{tr}, \bar{\varepsilon}^p\right) = \left|\sigma_1^{tr}\right| - \sigma_0\left(\frac{E\bar{\varepsilon}^{p,tr}}{\alpha\sigma_0} + r^m\right)^{1/m}$$

if $f^{tr} \le 0$

Elastic step: set $(\bullet)_{(i+1)} = (\bullet)^{tr}$

Else

Plastic step: Proceed with return mapping algorithm (see Box 4)

End if

End while

Box 4 Return mapping algorithm for pipe section used in Box 3

1. solve $\Delta\bar{\varepsilon}^p$:

$$f(\sigma_1, \bar{\varepsilon}^p) = |\sigma_1| - \sigma_0\left(\frac{E\bar{\varepsilon}^p}{\alpha\sigma_0} + r^m\right)^{1/m} = 0 \Rightarrow$$

$$f(\sigma_1, \bar{\varepsilon}^p) = \left|\sigma_1^{tr}\right| - E\Delta\bar{\varepsilon}^p - \sigma_0\left(\frac{E\bar{\varepsilon}^p}{\alpha\sigma_0} + r^m\right)^{1/m} = 0 \Rightarrow$$

$$f(\sigma_1, \bar{\varepsilon}^p) = \left|\sigma_1^{tr}\right| - E\Delta\bar{\varepsilon}^p - \sigma_0\left[\frac{E(\bar{\varepsilon}^p{}_t + \Delta\bar{\varepsilon}^p)}{\alpha\sigma_0} + r^m\right]^{1/m} = 0$$

$$f(\sigma_1, \bar{\varepsilon}^p) = \left|\sigma_1^{tr}\right| - E\Delta\bar{\varepsilon}^p - \sigma_0\left[\frac{E(\bar{\varepsilon}^{p,tr} + \Delta\bar{\varepsilon}^p)}{\alpha\sigma_0} + r^m\right]^{1/m} = 0$$

solve $\Delta\bar{\varepsilon}^p$ (Newton iteration)

2. update strain and stress

$$\Delta\varepsilon_1^p = \Delta\bar{\varepsilon}^p \times \text{sign}\left(\sigma_1^{tr}\right)$$

$$\varepsilon_1^{p,(i+1)} = \varepsilon_1^{p,(i)} + \Delta\varepsilon_1^p$$

$$\bar{\varepsilon}^p = \bar{\varepsilon}^{p(i)} + \Delta\bar{\varepsilon}^p$$

$$\sigma_1 = EkRy' + Eb - E\varepsilon_1^p$$

3.2 | FEA-based validations

To validate the numerical procedures presented in the last section for calculating structural strain from the governing equations given in Section 3.1, commercial FE software ABAQUS[31] is used here for computing structural strain in a plate section modelled as a 2D plane-strain problem, as shown in Figure 6A. The remote loading condition is prescribed as $\sigma_m = 0.6\sigma_0$ and $\sigma_b = 0.25\sigma_0$. Both stress and structural strain distributions calculated during loading and after unloading are compared in Figure 6B, C, respectively, between FEA solutions and the results obtained using the analytical formulations developed in this study. Note that the material considered here is ASTM A302-B steel, and the corresponding Ramberg-Osgood material parameter is documented in Qian.[32] In the modified Ramberg-Osgood material model, the normalized proportional limit of the material is found to be 0.7, ie, $r = 0.7\sigma_0$. An applied remote traction stress is at $\sigma_m + \sigma_b = 0.85\sigma_0 > 0.7\,\sigma_0$ so that a certain extent of plastic deformation is expected. It should be emphasized here that σ_0 in Ramberg-Osgood equation is a reference stress and typically greater than the yield strength σ_Y of the material.

The element type used here for performing ABAQUS based FE analysis is 4-node bilinear plane strain elements with hybrid integration scheme for constant pressure, ie, "CPE4H" which is specifically formulated for large plastic strain problems. As shown in Figure 6, the analytically formulated structural strain method implemented in the form of numerical algorithms developed in this study shows an excellent agreement with the FEA results, validating both the analytical formulations and numerical procedures. The finite element results in total strain in Figure 6B further validate the appropriateness of the "through thickness linear deformation gradient" assumption because there is no linear strain gradient constraints imposed in obtaining the finite element solutions.

As for structural strain calculations for a pipe section, beam element type "B21" in ABAQUS is used here. Because of the anticipated extent of plastic deformation involved, a total of 56 additional integration points beyond the default value of 25 were introduced for a better resolution of beam section plastic deformation behaviour, as illustrated in Figure 7A. The material considered in the pipe section is identical to the one used in the plate section problem shown in Figure 6. The results are

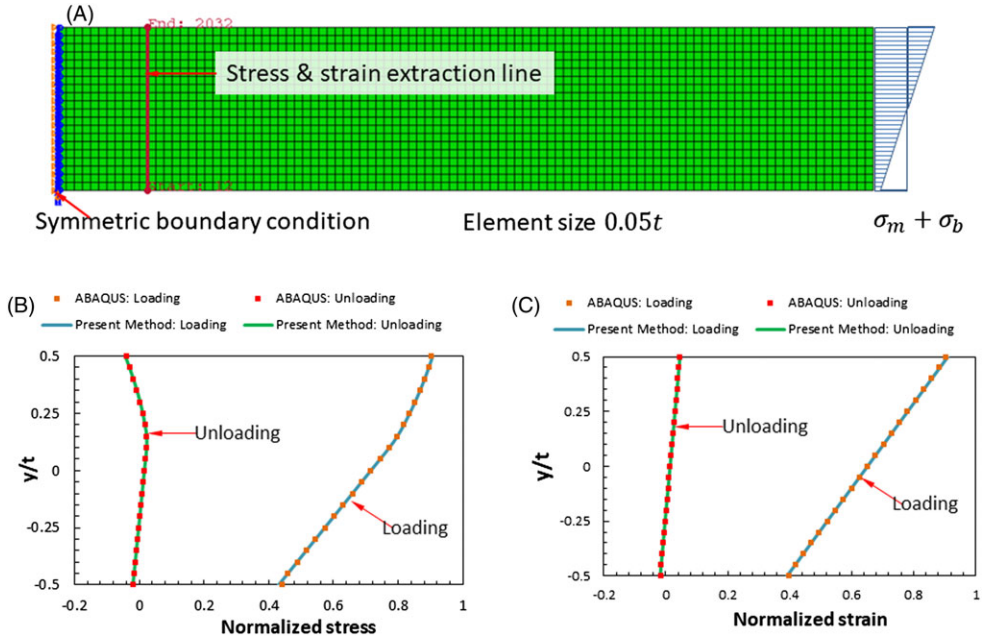

FIGURE 6 Comparison of FEA results with the results obtained by the present analytical formulation for a plate section. A, Finite element model used. B, Comparison of stress distributions. C, Comparison of structural strains [Colour figure can be viewed at wileyonlinelibrary.com]

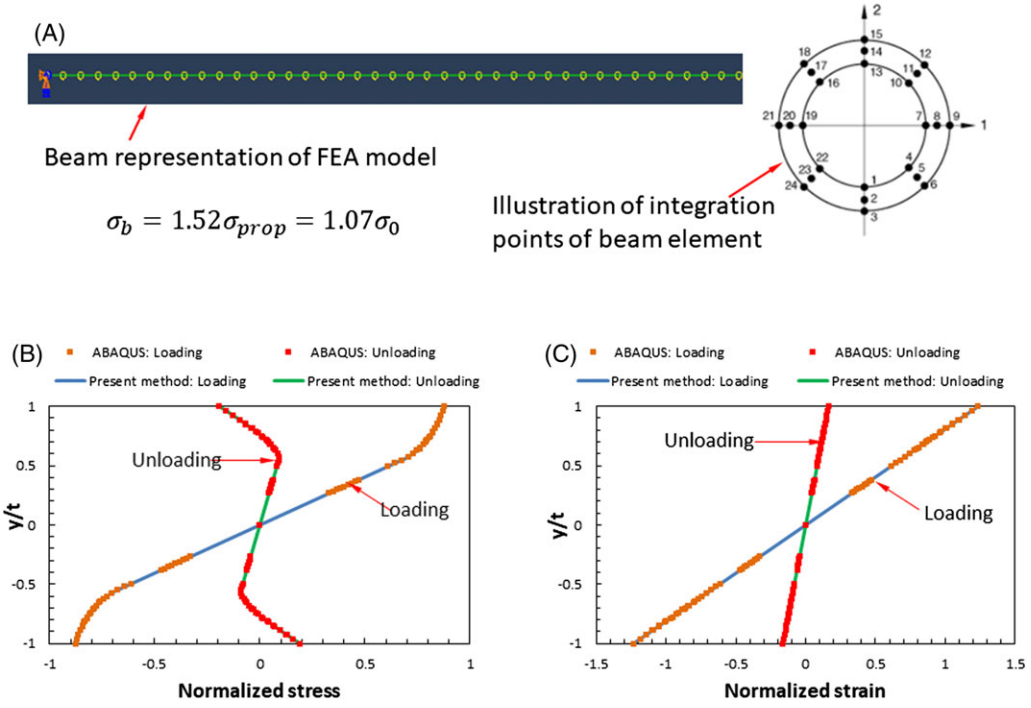

FIGURE 7 Comparison of FE results with the results obtained using the analytical formulations developed in this paper for a pipe section: A, Beam element model representing a pipe section, B, comparison of stress distributions, and C, comparison of structural strains [Colour figure can be viewed at wileyonlinelibrary.com]

compared in Figure 7B in stresses and Figure 7C in strains with the results obtained through the analytical formulation developed in this study. Again, an excellent agreement between the 2 independent solutions can be seen in both Figure 7B, C, validating the present approach for applications in pipe sections.

3.3 | Application in fatigue test data correlation

Three independent sets of fatigue test data of welded components with fatigue lives spanning both high-cycle and low-cycle regimes are considered here. The first set

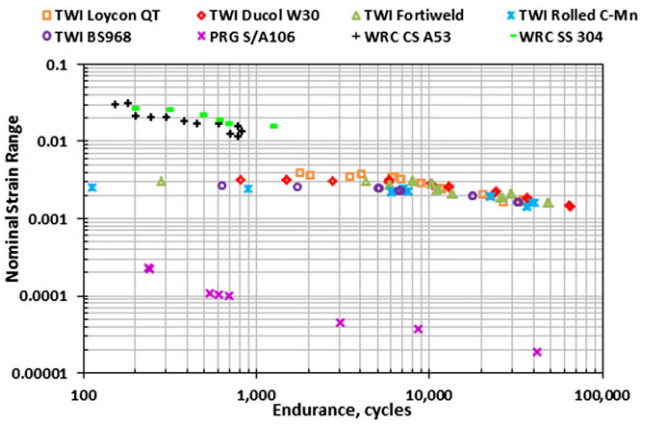

FIGURE 8 Correlation of fatigue test data using measured strain (PRG and WRC) and nominal strain (TWI) [Colour figure can be viewed at wileyonlinelibrary.com]

represents filleted welded plate-gusset specimen tests performed by The Welding Institute (TWI),[33] the second set contain girth-welded pipes sponsored by Welding Research Council (WRC),[18] and the third involves fatigue tests of girth welded pipe to nozzle fitting connections by Paulin Research Group (PRG).[34] Materials used in these tests involve high-strength low alloy steels, low carbon steels, and 304 stainless steel. Details can be found in their reports. It should also be noted that the gusset-on-plate specimen tests by TWI[33] were carried out under load-controlled conditions, while the tests by PRG[34] and WRC[18] were performed under displacement-controlled conditions. Nominal strain measurements are available for tests performed by PRG and WRC, while only nominal stress range is available for tests performed by TWI. All 3 sets of fatigue test results are plotted in Figure 8 in nominal strain range versus cycle to failure. Note that because of the lack of measured strains in TWI's tests, the nominal strains are calculated based on nominal stress ranges provided by the nominal stress ranges divided by steel Young modulus.

Because of differences in measurement locations as well as calculated strains based on nominal stresses, the 3 sets of test data follow 3 separate trend lines, as expected. Furthermore, test data obtained under load-controlled conditions by TWI exhibit a "flattened off" region in low-cycle fatigue regime, which is a common feature when a stress-based parameter is used.

In contrast, once all these test data are plotted in structural strain parameter $\Delta\epsilon_s$ calculated from the analytical formulation given in Section 2, a single narrow and approximately straight band can be seen in Figure 9, covering data from very low-cycle fatigue regime (a few hundreds of cycles to failure) to a regime corresponding to high-cycle fatigue (at 10^5 cycles to failure). This suggests that the structural strain parameter serves as a good fatigue parameter for fatigue characterization in both low-cycle and high-cycle regimes. The effectiveness of the structural strain parameter in correlating both low-cycle and high-cycle fatigue data further substantiates the fact that fatigue damage is a strain-controlled phenomenon, rather than stress-controlled. Instead of using a notch strain-based parameter widely discussed in literature,[6,12,13] the present study introduces a cross section-based structural strain definition, which can be directly implemented for applications in complex structures and loading conditions. Further discussions, additional validations, as well as proposed implementation in codified procedures[35] will be presented in an ensuing paper.[36]

4 | DISCUSSIONS

4.1 | Plane stress versus plane strain conditions

Dong et al[21] first introduced the "structural strain" method for evaluating low-cycle fatigue behaviours of welded components. For simplicity, they assumed plane stress conditions to obtain closed form solutions of structural strain as a correction to elastically calculated traction structural stresses. As a result, the applicability of their structural strain solutions is restricted to small

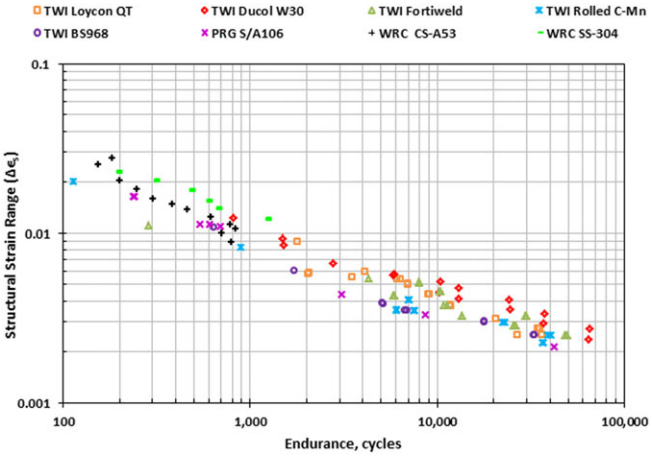

FIGURE 9 Correlation of fatigue test data from PRG, TWI, and WRC using structural strain range calculated using the formulations developed in this study [Colour figure can be viewed at wileyonlinelibrary.com]

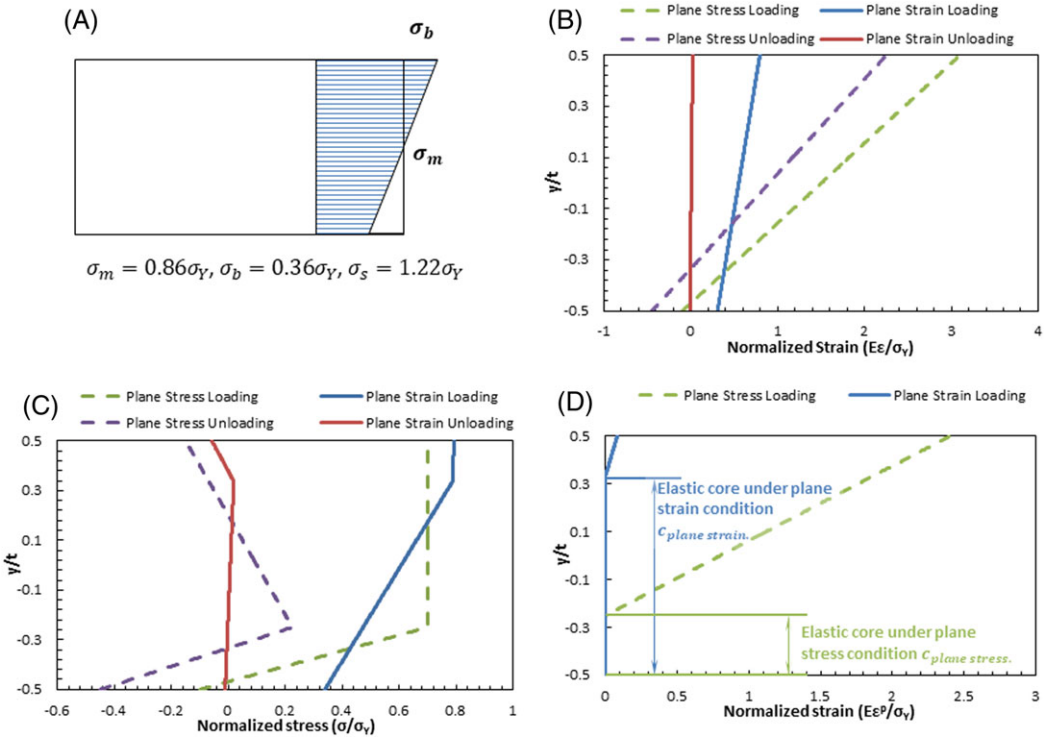

FIGURE 10 Comparison of section behaviour under plain stress and plain strain condition: A, load definition, B, comparison of total strain distribution, C, comparison of normal stress distribution, and D, comparison of plastic strain distribution [Colour figure can be viewed at wileyonlinelibrary.com]

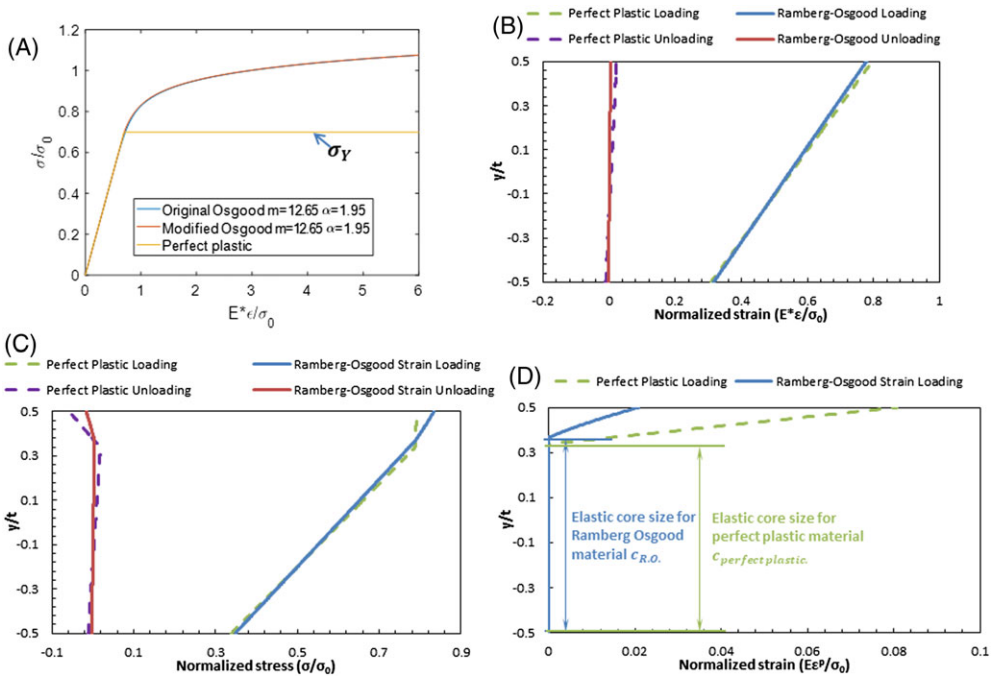

FIGURE 11 Comparison of section behaviour with and without strain hardening consideration: A, stress-strain curve comparison, A, comparison of structural strain (total strain) distribution, C, comparison of normal stress distribution, and D, comparison of plastic strain distribution [Colour figure can be viewed at wileyonlinelibrary.com]

scale yielding conditions. For most structural applications, plane-strain conditions should be more appropriate when a plate cross section is considered as discussed in this paper. With the new developments presented in this paper, plane-strain conditions can now be treated with ease. Then, it should be informative to examine

the applicability of the 2 conditions in structural strain calculations.

Consider a plate through-thickness section subjected to remote membrane and bending stresses of $\sigma_m = 0.86\sigma_Y$ and $\sigma_b = 0.36\sigma_Y$, respectively, as shown in Figure 10A. At first, elastic perfectly plastic material model is considered. Figure 10B shows the comparison of the structural strain results between the 2 cases, both during loading and after unloading. As can be clearly seen, the calculated structural strains under plane-stress conditions are about 3 times that under plane-strain conditions. Such a large difference in structural strain results can be readily explained by examining Figure 10C in differences in resulting stress distributions and Figure 10D in elastic core sizes. The extent of plastic deformation under plane stress conditions is so large, with an elastic core be reduced to only about 20% of the plate thickness or $0.2t$, while under plane strain conditions, the corresponding elastic core size still remains at $0.8t$, which is 4 times bigger than that under plane stress conditions. The results in Figure 10 strongly suggest that that plane strain conditions should be used in general for computing structural strains for performing low-cycle fatigue evaluation of plate structures.

4.2 | Effect of material strain hardening

Consider the same plate section examined in Figure 10, subjected to remote loading conditions corresponding to $\sigma_m = 0.6\sigma_0$ and $\sigma_b = 0.25\sigma_0$, in which σ_0 is the reference stress. And Ramberg-Osgood parameters used here are $\alpha = 1.95$, $m = 12.65$, and $\sigma_{prop} = 0.7\sigma_0$. For the case with elastic perfectly plastic model, yield stress of the material is set as $\sigma_Y = 0.7\sigma_0$. Plane strain conditions are considered in both cases.

The structural strain results for the 2 cases are compared in Figure 11B, showing rather insignificant differences both at loading and after unloading stage. The local stress results show a more noticeable difference between the 2 cases in Figure 11C in a region corresponding $y > 0.3t$ in which both cases experience plastic deformation. Figure 11D shows that the peak local plastic strain value for the case of elastic perfectly plastic material is about 4 times greater than that for the case of Ramberg-Osgood material while the difference in elastic core size between the 2 is only about 4%, ie, being negligible. Both the structural strain results in Figure 11B and elastic core size results shown in Figure 11D seem to confirm the postulation by Dong et al[21] that the structural strain is dominated by elastic core size. The results also suggest that if Ramberg-Osgood material parameters are not available for a material of interest, the use of elastic perfectly plastic model can still yield a reasonable estimation of structural strain for low-cycle fatigue evaluation purpose.

5 | CONCLUSIONS

In this paper, an analytically formulated structural strain method is presented for fatigue evaluation of welded components:

- A modified Ramberg-Osgood power law hardening model is developed to incorporate nonlinear material hardening behaviours. The modified Ramberg-Osgood power law hardening model enables a consistent partitioning of elastic and plastic strain increments during both loading and unloading, which enables people to determine both structural strain and elastic core size numerically.
- The new structural strain method is cast in 2 forms for facilitating fatigue evaluation of 2 major forms welded structures used in industry: 1 is for structural strain determination with respect to a through-thickness section in plate structures and the other for structural strain determination with respect to pipe cross section in piping systems.
- The structural strain is defined as the linearly distributed total strain (linear deformation gradient) on the cross section, consistent with the "plane sections remain plane" assumption in the context of structural mechanics.
- A set of robust numerical procedures are presented for solving the analytically formulated structural strain expressions.
- The structural strain-based fatigue parameter proposed has been shown effective in correlating some well-known low-cycle and high-cycle fatigue test data from 3 independent laboratories, ranging from mild steel to high-strength steel weldments, from gusset-to-plate welded plate connections to pipe girth welds.

With the new developments presented in this paper, the structural strain method can be used as a postprocessing procedure applied to linear elastic traction structural stresses obtained at a given plate or pipe cross section by the mesh-insensitive structural stress method adopted by ASME Div 2 since 2007, which can be used for complex structures and loading conditions. The resulting master E-N curve serves as a natural extension of the master S-N curve which is dominated by high-cycle fatigue test data into low-cycle regime, as shown in Figure 9, which will be further substantiated by an ensuring paper by the same authors.[36]

ACKNOWLEDGEMENTS

The authors gratefully acknowledge the support of this work in part by ONR Grant No. N00014-10-1-0479 at UNO and a

National Research Foundation of Korea (NRF) grant funded by the Korean government (MEST) through GCRC-SOP at University of Michigan under Project 2-1: Reliability and Strength Assessment of Core Parts and Material System. P. Dong also acknowledges partial financial support made possible by Traction Power National Key Laboratory Open Competition Grant No. TPL 1605.

ORCID

Xianjun Pei http://orcid.org/0000-0001-5282-0607

REFERENCES

1. Dong P. A structural stress definition and numerical implementation for fatigue analysis of welded joints. *International Journal of Fatigue*. 2001;23(10):865-876.
2. Code of practice for fatigue design and assessment of steel structures. BS7608, British Standards Institution, 1993.
3. Design of steel structures—part 1-1. ENV 1993-1-1. Eurcode 3, European Committee for Standardization, Brussels, 1992.
4. Hobbacher A. *Fatigue Design of Welded Joints and Components: Recommendations of IIW Joint Working Group XIII–XV*. Abington, Cambridge: Abington Publishing; 1996.
5. Hobbacher A. Basic philosophy of the new IIW recommendations on fatigue design of welded joints and components. *Welding in the World*. 1997;39(5):272-278.
6. Radaj D. Review of fatigue strength assessment of non-welded and welded structures based on local parameters. *Int J Fatigue*. 1996;18(3):153-170.
7. Lawrence FV, Mattos RJ, Higashida Y, Burk JD. Estimating the fatigue crack initiation life of welds. *ASTM STP*. 1978;648:134-158.
8. Dong P, Hong JK, De Jesus AM. Analysis of recent fatigue data using the structural stress procedure in ASME div 2 rewrite. *J Press Vessel Technol*. 2007;129(3):355-362.
9. AASHTO. LRFD. *AASTO LRFD Bridge Design Specifications*. 3rd ed. D.C.: Washington; 2004.
10. Zhang G, Richter B. A new approach to the numerical fatigue-life prediction of spot-welded structures. *Fatigue Fract Eng Mater Struct*. 2000;23(6):499-508.
11. ZHANG, GENBAO, Martin EIBL, and Sumanjit SINGH. Methods of predicting the fatigue lives of laser-beam welded lap welds subjected to shear stresses. *Weld Cut* 2 (2002): 96–103.
12. Morgenstern C, Sonsino CM, Hobbacher A, Sorbo F. Fatigue design of aluminium welded joints by the local stress concept with the fictitious notch radius of rf= 1 mm. *Int J Fatigue*. 2006;28(8):881-890.
13. Schmidt H, Baumgartner J, Melz T. Fatigue assessment of joints using the local stress field. *Materialwissenschaft Und Werkstofftechnik*. 2015;46(2):145-155.
14. Dong P, Hong JK, Cao Z. Stresses and stress intensities at notches: 'anomalous crack growth' revisited. *Int J Fatigue*. 2003;25(9–11):811-825.
15. Mei J, Dong P. An equivalent stress parameter for multi-axial fatigue evaluation of welded components including non-proportional loading effects. *Int J Fatigue*. 2017;101:297-311.
16. Dong P, Cao Z, Hong JK. Low-cycle fatigue evaluation using the weld master SN curve. In: *ASME 2006 pressure vessels and piping/ICPVT-11 conference*. American Society of Mechanical Engineers; 2006, January:237-246.
17. Markl ARC. Fatigue tests of piping components. *Trans ASME*. 1952;74:287-303.
18. Scavuzzo, R.J., Srivatsan, T.S., and Lam, P.C., Fatigue of butt-welded pipe, Report 1 in Fatigue of Butt-Welded Pipe and Effect of Testing Methods, *Weld Res Counc Bull* 433, July 1998.
19. Dong P, Yang X. A master SN curve representation of subsea umbilical tube weld fatigue data. In: *ASME 2010 29th international conference on ocean, offshore and Arctic engineering*. American Society of Mechanical Engineers; 2010, January:177-184.
20. Gas Transmission and Distribution Piping Systems, ASME B31.8–2003, American Society of Mechanical Engineers, 2003
21. Dong P, Pei X, Xing S, Kim MH. A structural strain method for low-cycle fatigue evaluation of welded components. *Int J Press Vessel Pip*. 2014;119:39-51.
22. Pei X, Wang W, Dong P. An analytical-based structural strain method for low cycle fatigue evaluation of girth-welded pipes. In: *ASME 2017 pressure vessels and piping conference*. American Society of Mechanical Engineers; 2017, July: V03BT03A015-V03BT03A015.
23. Dong P, Pei X, Xing S. A structural strain method for fatigue evaluation of welded components. In: *ASME 2014 33rd international conference on ocean, offshore and Arctic engineering*. American Society of Mechanical Engineers; 2014, June: V005T03A037-V005T03A037.
24. American Society of Mechanical Engineers, 1997, ASME Boiler and Pressure Vessel code, Section 3, Rules for Construction of Nuclear Power Plant Components, NB, Class 1 Components and Section VIII, Rules for Construction of Pressure Vessels, Division 2-Alternate Rules.
25. Ramberg, Walter, and William R. Osgood. Description of stress-strain curves by three parameters. (1943).
26. Basan R, Franulović M, Prebil I, Kunc R. Study on Ramberg-Osgood and Chaboche models for 42CrMo4 steel and some approximations. *J Constr Steel Res*. 2017;136:65-74.
27. Liu N, Jeffers AE. Adaptive isogeometric analysis in structural frames using a layer-based discretization to model spread of plasticity. *Comput Struct*. 2018;196:1-11.
28. Zappalorto M, Maragoni L. Nonlinear mode III crack stress fields for materials obeying a modified Ramberg-Osgood law. *Fatigue Fract Eng Mater Struct*. 2018;41(3):708-714.
29. Qian L. Principle of complementary energy. *Sci China Ser A*. 1950;1(2):449-456.
30. Simo JC, Hughes TJ. *Computational Inelasticity*. 7 Springer Science & Business Media; 2006.
31. Hibbit Karlson, Sorensen Inc, ABAQUS Version 6.12, 2003.
32. James LA. Ramberg-Osgood strain-hardening characterization of an ASTM A302-B steel. *J Press Vessel Technol*. 1995;117(4):341-345.

33. Harrison, J. D. Fatigue performance of welded high strength steels, a compendium of reports from sponsored research programme. The Welding Institute, Abington Hall, Arbinton, Cambridge CBI 6AL, England (1974).

34. Hinnant, Chris, and Tony Paulin. Experimental evaluation of the markl fatigue methods and ASME piping stress intensification factors. ASME 2008 Pressure vessels and piping conference. American Society of Mechanical Engineers, 2008.

35. Osage DA, Dong P, Spring D. Fatigue assessment of welded joints in API 579-1/ASME FFS-1 2016-existing methods and new developments. *Procedia Engineering*. 2018;213:497-538.

36. Pei, X and Dong, P, Application of structural strain method for fatigue evaluation of welded components of different materials (to be submitted)

How to cite this article: Pei X, Dong P. An analytically formulated structural strain method for fatigue evaluation of welded components incorporating nonlinear hardening effects. *Fatigue Fract Eng Mater Struct*. 2019;42:239–255. https://doi.org/10.1111/ffe.12900

APPENDIX A

IDEA OF MODIFIED RAMBERG-OSGOOD EQUATION

Figure A1 demonstrates the idea of modified Ramberg-Osgood equation: When $\sigma = \sigma_{pro}$, according to the original Ramberg-Osgood equation, the total strain is $\varepsilon = \sigma_{pro}/E + \alpha\sigma_0 r^m/E$ (here $r = \sigma_{pro}/\sigma_0$). However, by definition, below material proportional limit σ_{pro}, there should be only elastic strain, ie, $\varepsilon = \sigma_{pro}/E$. In the modified Ramberg-Osgood equation, the total strain is offset by $\alpha\sigma_0 r^m/E$, when the stress is beyond material proportional limit. According to modified Ramberg-Osgood equation, there is no nonlinear term when applied stress is less then proportional limit σ_{pro}.

APPENDIX B

PROOF OF EQUATION (27)

Here, a time step from t to $t + \Delta t$ is considered. And in what follows, all quantities are taken to be those at the end of a time step, ie, at $t + \Delta t$, unless specifically stated. So, the stress at $t + \Delta t$ is just noted as $\boldsymbol{\sigma}$ rather than $\boldsymbol{\sigma}_{t+\Delta t}$, for simplicity. The quantities at the beginning of a time step is described using a subscript t, for example, stress at beginning of the time step is noted as $\boldsymbol{\sigma}_t$.

As given in Equations 11 and 12, stress-strain relationship of small strain theory is as follows.

$$\sigma = 2G\varepsilon^e + \lambda Tr(\varepsilon^e)\mathbb{I}$$
$$\lambda = \frac{E\nu}{(1+\nu)(1-2\nu)} \tag{A1}$$

The strain decomposition in the time step is given by:

$$\varepsilon^e = \varepsilon^e_t + \Delta\varepsilon^e = \varepsilon^e_t + \Delta\varepsilon - \Delta\varepsilon^p \tag{A2}$$

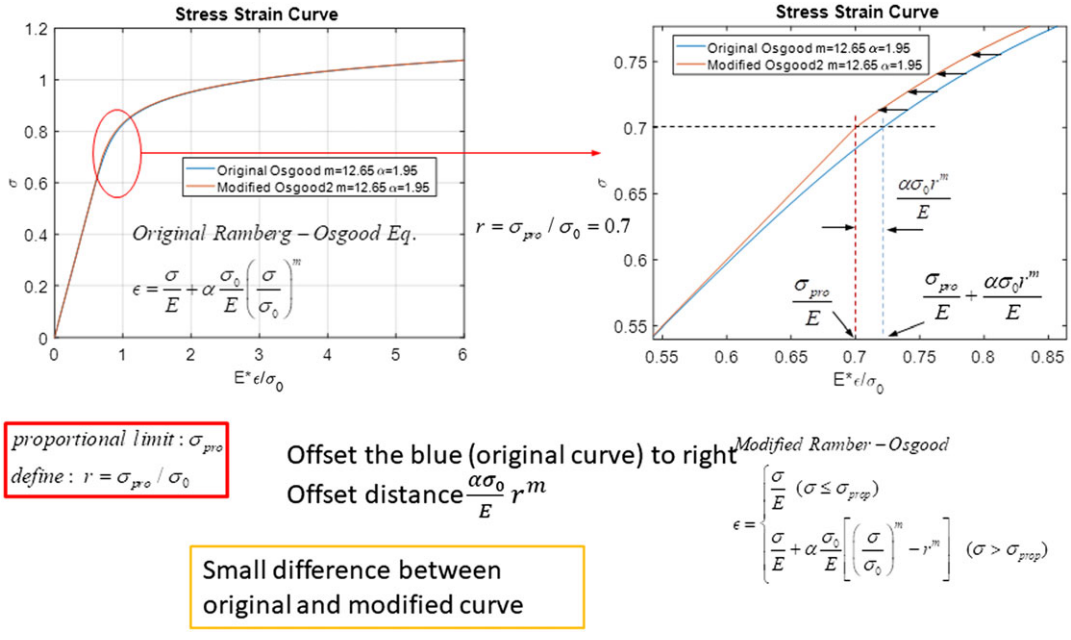

FIGURE A1 Illustration of idea of modified Ramberg-Osgood equation [Colour figure can be viewed at wileyonlinelibrary.com]

From A1 and A2, we have:

$$\begin{aligned}\sigma &= 2G(\varepsilon^e + \Delta\varepsilon - \Delta\varepsilon^p) + \lambda Tr(\varepsilon^e + \Delta\varepsilon - \Delta\varepsilon^p)\mathtt{I} \\ \sigma &= 2G(\varepsilon^e + \Delta\varepsilon) + \lambda Tr(\varepsilon^e + \Delta\varepsilon)\mathtt{I} - 2G\Delta\varepsilon^p\end{aligned} \tag{A3}$$

Here in Eq. A3, incompressibility for plasticity condition is used, which is.

$$Tr(\Delta\varepsilon^p) = \Delta\varepsilon_1^p + \Delta\varepsilon_2^p + \Delta\varepsilon_3^p = 0 \tag{A4}$$

Define trial stress $\boldsymbol{\sigma}^{tr}$ as:

$$\sigma^{tr} = 2G(\varepsilon^e + \Delta\varepsilon) + \lambda Tr(\varepsilon^e + \Delta\varepsilon)\mathtt{I} \tag{A5}$$

Also because of incompressibility condition,

$$\begin{aligned}Tr(\sigma) &= Tr[2G(\varepsilon^e + \Delta\varepsilon) + \lambda Tr(\varepsilon^e + \Delta\varepsilon)\mathtt{I} - 2G\Delta\varepsilon^p] \\ &= Tr[2G(\varepsilon^e + \Delta\varepsilon) + \lambda Tr(\varepsilon^e + \Delta\varepsilon)\mathtt{I}] - 2GTr(\Delta\varepsilon^p) \\ &= Tr[2G(\varepsilon^e + \Delta\varepsilon) + \lambda Tr(\varepsilon^e + \Delta\varepsilon)\mathtt{I}] = Tr(\sigma^{tr})\end{aligned} \tag{A6}$$

From A3 and A5:

$$\sigma = \sigma^{tr} - 2G\Delta\varepsilon^p \tag{A7}$$

And as already given by Equations 16 and 25, for von-Mises yield criteria, $\Delta\boldsymbol{\varepsilon}^p$ is given by:

$$\Delta\varepsilon^p = \frac{3}{2}\Delta\bar{\varepsilon}^p\frac{\sigma'}{\sigma_e} \tag{A8}$$

Same as before, σ_e is the von-Mises and $\boldsymbol{\sigma}'$ is deviatoric stress given by:

$$\sigma' = \sigma - \frac{1}{3}Tr(\sigma)\mathtt{I} \tag{A9}$$

Here, $\boldsymbol{I}$ is the second-order isotropic tensor (kronecker delta). Combine A7 and A8, we have

$$\begin{aligned}\sigma^{tr} - 2G\Delta\bar{\varepsilon}^p\frac{3\sigma'}{2\sigma_e} = \sigma &= \sigma' + \frac{1}{3}Tr(\sigma)\mathtt{I}\sigma^{tr} - \frac{1}{3}Tr(\sigma)\mathtt{I} \\ &= \sigma' + 3G\Delta\bar{\varepsilon}^p\frac{\sigma'}{\sigma_e}\end{aligned} \tag{A10}$$

Bear A6 in mind, A10 can be rewritten as:

$$\begin{aligned}&\sigma^{tr} - \frac{1}{3}Tr(\sigma^{tr})\mathtt{I} = \sigma' + 3G\Delta\bar{\varepsilon}^p\frac{\sigma'}{\sigma_e}\sigma^{tr'} \\ &= \left(1 + 3G\frac{\Delta\bar{\varepsilon}^p}{\sigma_e}\right)\sigma'\end{aligned} \tag{A11}$$

Here, $\boldsymbol{\sigma}^{tr'}$ is deviatoric trial stress, and from A11

$$\frac{3}{2}\sigma^{\mathrm{tr}'}:\sigma^{\mathrm{tr}'} = \left(1 + 3G\frac{\Delta\bar{\varepsilon}^p}{\sigma_e}\right)^2\frac{3}{2}\sigma':\sigma' \tag{A12}$$

Notice that by the definition of von-Mises, one can write

$$\sigma_e^2 = \frac{3}{2}\sigma':\sigma' \tag{A13}$$

Leading to

$$\left(\sigma_e^{tr}\right)^2 = \left(1 + 3G\frac{\Delta\bar{\varepsilon}^p}{\sigma_e}\right)^2\sigma_e^2 \tag{A14}$$

And finally reaches to Equation 27

$$\begin{aligned}\sigma_e^{tr} &= \left(1 + 3G\frac{\Delta\bar{\varepsilon}^p}{\sigma_e}\right)\sigma_e \\ \sigma_e &= \sigma_e^{tr} - 3G\Delta\bar{\varepsilon}^p\end{aligned} \tag{A15}$$

APPENDIX C

PROOF OF EQUATION 28

According to elastic stress-strain relationship and definition of trial stress:

$$\begin{aligned}\sigma_1 &= E(\varepsilon_1 - \varepsilon_1^p) = E\left(\varepsilon_1 - \varepsilon_{1,t}^p\right) + E\left(\varepsilon_{1,t}^p - \varepsilon_1^p\right) \\ \sigma_1 &= \sigma_1^{tr} - E\Delta\gamma \times \mathrm{sign}(\sigma_1)\end{aligned} \tag{A16}$$

Notice that

$$\sigma_1 = |\sigma_1|\,\mathrm{sign}(\sigma_1) \tag{A17}$$

Eq. A16 can be rewritten as:

$$\begin{aligned}|\sigma_1|\,\mathrm{sign}(\sigma_1) &= \left|\sigma_1^{tr}\right|\mathrm{sign}\left(\sigma_1^{tr}\right) - E\Delta\gamma \times \mathrm{sign}(\sigma_1) \\ [|\sigma_1| + E\Delta\gamma]\,\mathrm{sign}(\sigma_1) &= \left|\sigma_{n+1}^{trial}\right|\mathrm{sign}\left(\sigma_{n+1}^{trial}\right)\end{aligned} \tag{A18}$$

Because $\Delta\gamma$ is greater or equal to zero by definition of plastic multiplier,

$$\begin{aligned}&[|\sigma_1| + E\Delta\gamma] \geq 0 \\ &\left|\sigma_{n+1}^{trial}\right| \geq 0\end{aligned} \tag{A19}$$

Combining A18 and A19, we have:

$$\mathrm{sign}(\sigma_1) = \mathrm{sign}\left(\sigma_1^{tr}\right) \tag{A20}$$